International Journal of Thermal Sciences 75 (2014) 171–183

Contents lists available at ScienceDirect

International Journal of Thermal Sciences

journal homepage: www.elsevier.com/locate/ijts

Numerical simulation of modulated heat transfer tube in laminar flow regime

Zhen Cao [a], Jinliang Xu [a,b,*], Dongliang Sun [b,**], Jian Xie [b], Feng Xing [b], Qicheng Chen [b], Xiaodong Wang [b]

[a] State Key Laboratory of Alternate Electrical Power System with Renewable Energy Sources, North China Electric Power University, Beijing 102206, China
[b] The Beijing Key Laboratory of Multiphase Flow and Heat Transfer, North China Electric Power University, Beijing 102206, China

ARTICLE INFO

Article history:
Received 18 May 2013
Received in revised form
14 July 2013
Accepted 12 August 2013
Available online

Keywords:
Flow field modulation
Modulated heat transfer tube
Laminar flow
Heat transfer enhancement

ABSTRACT

The flow field modulation concept was proposed. A mesh cylinder was suspended in a tube, dividing the tube cross section into an annular region and a core region. The invention is called the modulated heat transfer tube (MHTT). The numerical simulation was performed in laminar flow regime at constant heat flux boundary condition with water as the working fluid. An equal flow area criterion was proposed for the conversion of 3D to 2D mesh pores. The non-uniform grids link micron scale of mesh pores with meter scale of tube. The results show double-peak velocity distribution over tube cross section. The near wall region has larger velocity and velocity gradient, accounting for the heat transfer enhancement mechanism. For any specific Reynolds number, there is a critical length beyond which heat transfer is deteriorated. Therefore, a set of short mesh cylinders was suspended in the tube. The configuration is called the improved modulated heat transfer tube (IMHTT). It is shown that the IMHTT ensures significant heat transfer enhancement over the whole tube length. This study provides a new enhancement mechanism and tube configuration for heat transfer, having a wide engineering application potential.

1. Introduction

Heat transfer tubes are widely used in many energy conversion and power generation systems. Heat transfer in tubes, with various geometry shapes, dimensions and material has been investigated by more than one century. According to the thermodynamic law, the exergy efficiency is increased by decreasing temperature differences across the two sides of the tube. This requires significantly higher heat transfer coefficients with acceptable pumping power.

The worldwide energy shortage and environment problems demand the energy utilization efficiency to be increased for fossil energy systems. Meanwhile, renewable energy such as solar energy, ocean energy etc. has been put into use. Miniaturization of heat exchangers increases system efficiencies and decreases investment cost. Under many situations, one needs to extract low grade energy from extremely low temperature resource. An example was cited from Ref. [1]. A heat exchanger for an ocean thermal energy conversion (OTEC) plant requires a heat transfer surface area in the order of 10^4 m^2/MW.

The classical fluid mechanics tells us that the non-slip boundary condition on wall is acceptable to predict flow and heat transfer behavior in tubes. This implies a stationary thin fluid layer on the wall. Besides, velocity and velocity gradient near the wall are limited, no matter for laminar or turbulent flows. Such flow behavior directly limits the temperature gradient near the wall to determine the heat transfer coefficient. Besides, after a long time operation of heat exchangers, the thermal resistance is increased due to fouling. This problem becomes more serious when a system is operating at dirty environment or an impurity working fluid flows in tubes. Conventionally, heat transfer performance can be improved by introducing a disturbance in fluid flow (breaking the viscous and thermal boundary layers).

Various techniques have been proposed for heat transfer enhancement in the literature. These can be found in consecutive review articles such as Dewan et al. [1] and Liu and Sakr [2], etc. Heat transfer tubes with many kinds of inserts such as twisted tape, wire coil, swirl flow generator, etc. enhance the thermal efficiency. The twisted tape inserts are popular researched and used to strengthen the heat transfer efficiency [3–8]. Twisted tape inserts perform better in laminar flow regime than in turbulent flow regime. But other several passive techniques such as ribs, conical

* Corresponding author. State Key Laboratory of Alternate Electrical Power System with Renewable Energy Sources, North China Electric Power University, Beijing 102206, China. Tel./fax: +86 10 61772268.
** Corresponding author. Tel./fax: +86 10 61772268.
E-mail addresses: xjl@ncepu.edu.cn (J. Xu), dlsun@ncepu.edu.cn (D. Sun).

1290-0729/$ – see front matter © 2013 Elsevier Masson SAS. All rights reserved.
http://dx.doi.org/10.1016/j.ijthermalsci.2013.08.006

Nomenclature

A	flow area of the square mesh pores, m^2
A'	flow area of the stripe-type mesh pores, m^2
BT	bare tube
C_p	specific heat, J/kg K
D	bare tube diameter, m
D_m	mesh cylinder diameter, m
D_o	outer tube diameter, m
g	gravity acceleration ($g = 9.81$), m/s^2
IMHTT	improved modulated heat transfer tube
L	bare tube length, m
L_b	bare tube section length for the modulated heat transfer tube, m
$L_{b'}$	distance between two neighboring mesh cylinder, m
L_m	modulated flow section length for the modulated heat transfer tube, m
$L_{m'}$	a single short mesh cylinder length for the improved modulated heat transfer tube, m
L_t	the transition flow length, m
MHTT	modulated heat transfer tube
Nu_{ave}	average Nusselt number
Nu_x	local Nusselt number
p	pressure, pa
q	heat flux, W/m^2
q_w	the heat flux added to the wall, W/m^2
r	radial coordinate, m
Re	Reynolds number
T_f	the fluid temperature, K
$T_{f,ave}$	the average fluid temperature, K
T_{grid}	the temperature within the first fluid layer, K
T_{in}	the inlet temperature, K
T_{out}	the outlet temperature, K
T_w	the wall temperature, K
$T_{w,ave}$	the average wall temperature, K
T_{wo}	the outer wall temperature, K
u	the axial velocity, m/s
u_{ave}	the average velocity, m/s
u_w	the velocity on the wall, m/s
v	the radial velocity, m/s
w	square mesh pore width, m
w'	stripe-type mesh pore width, m
x	axial coordinate, m
y	first fluid layer thickness, m

Greek symbols

δ	square mesh wire thickness, m
δ'	stripe-type mesh wire thickness, m
λ	fluid thermal conductivity, W/m K
λ_w	tube wall thermal conductivity, W/m K
μ	dynamic viscosity, Pa s
ρ	density, kg/m^3
ϕ	enhanced heat transfer factor

Subscript

ave	average
b	bare tube
f	fluid
in	inlet
m	modulated tube
o	outer
out	outlet
w	tube wall
wo	outer tube wall
x	axial position

nozzle, and conical ring, etc. are generally more efficient in turbulent flow regime than in laminar flow regime [9–12].

The primary objective of this paper is to propose a new heat transfer tube. A mesh cylinder was suspended in the tube, dividing the tube into an annular region and a core region. The second objective of the paper is to verify the fresh idea by the numerical simulation together with the experimental data. The numerical results do show the larger velocity and velocity gradient near the wall. The numerical and experimental works are being continued. The future optimized heat transfer tube is expected to not only have significantly high heat transfer coefficients, but also delay the fouling, having wide engineering applications.

2. The modulated heat transfer tube

Fig. 1(a) shows the modulated heat transfer tube (MHTT). A mesh cylinder is suspended in a tube, dividing the tube cross section into an annular region and a core region. Supporting structures may be needed for a practical application. The mesh cylinder consists of a flat bottom mesh surface and a side circular mesh surface. Inside of the mesh cylinder is empty. When a fluid stream strikes the mesh cylinder, part of the flow rate enters the core region (mesh cylinder inside), but most of the flow rate flows in the annular region. The configuration creates larger velocity and velocity gradient near the wall in the annular region, which helps to enhance heat transfer. With flow evolution in the tube downstream, flow from the annular region to the core region is generated to decrease the velocity and velocity gradient in the annular region. The flow and heat transfer behavior in MHTT is thoroughly different from that in a concentric tube annular. The later configuration does not include mesh pores.

3. Numerical simulation and method

3.1. The 3D to 2D conversion of mesh pores

Numerical simulation of laminar flow and heat transfer in MHTT was performed. Initially, the 3D to 2D conversion of mesh cylinder was performed. MHTT is a multiscale system with three-levels of sizes: (1) micron scale of mesh pores; (2) miniature scale of the annular region; and (3) macroscale of the tube diameter and length (meter scale). Fig. 1(b) shows mesh cylinder with square mesh pores. The mesh cylinder diameter and length are recorded as D_m and L_m respectively. Mesh pores have a pore width of w and mesh wire thickness of δ. Assuming $D_m = 10.0$ mm, $L_m = 1000.0$ mm, $w = 165$ μm and $\delta = 85$ μm, the number of mesh pores attains 502,655 (million magnitude). Numerical simulation of such a huge number of mesh pores in micron scale is impossible at this stage. Thus a two-dimensional equivalent system should be developed and an equivalent criterion for mesh pores is necessary. Fig. 1(b) can be simplified to a 2D system by converting square mesh pores into stripe-type mesh pores (Fig. 1(c)), with a metal wire thickness of δ' and stripe-type mesh pore size of w'. At the mesh cylinder diameter of D_m and length of L_m, the total flow area of square mesh pores is

$$A = \frac{\pi D_m}{w+\delta} \times \frac{L_m}{w+\delta} \times w^2 \quad (1)$$

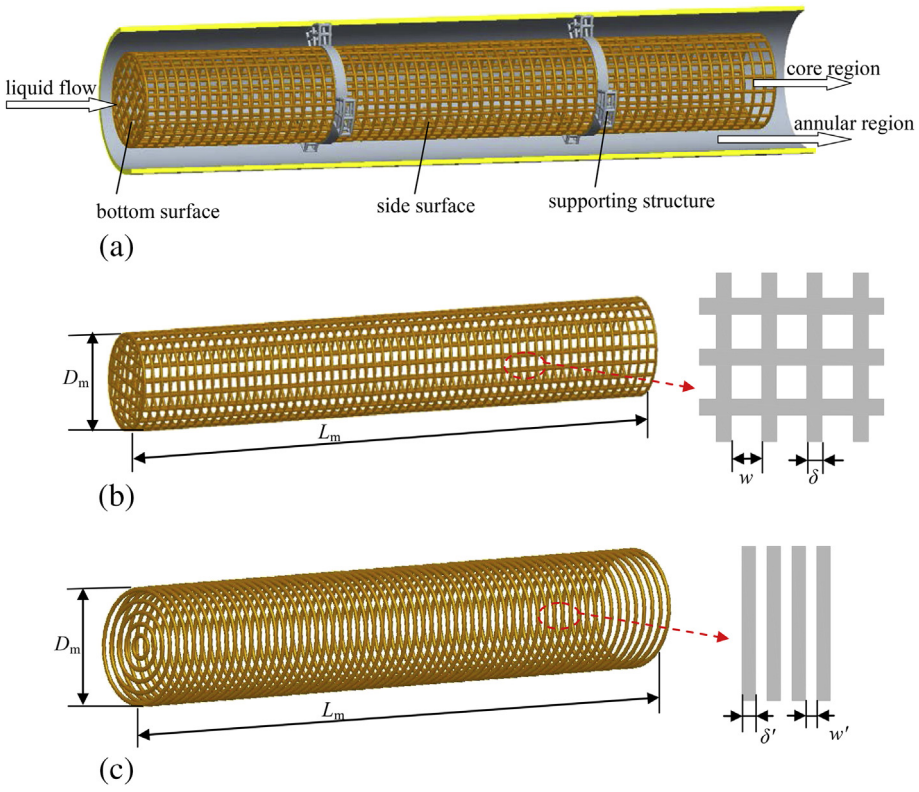

Fig. 1. The 3D to 2D conversion of mesh pores.

where the term $\pi D_m/(w+\delta)$ and $L_m/(w+\delta)$ are the number of mesh pores along the circumference direction and axial flow direction, respectively. Correspondingly, the stripe-type mesh pores have the flow area of

$$A' = \frac{L_m}{w'+\delta'} \times \pi D_m w' \tag{2}$$

The following equation exists due to $A = A'$.

$$\frac{w'}{w'+\delta'} = \left(\frac{w}{w+\delta}\right)^2 \tag{3}$$

During the conversion process, we keep $\delta' = \delta$. Thus w' can be obtained by Eq. (3). For practical application such as encountered in this paper, $w = 165$ μm, $\delta = 85$ μm, thus $\delta' = 85$ μm and $w' = 65$ μm for mesh pores with PPI = 100, where PPI refers to pores per inch.

3.2. Governing equations and boundary conditions

This is a steady, two-dimensional laminar flow and heat transfer problem. Both the flow and heat transfer are considered to be developing in the duct. The governing equations are

$$\nabla\cdot(\rho\vec{v}) = 0 \tag{4}$$

$$\nabla\cdot(\rho\vec{v}\vec{v}) = -\nabla p + \nabla\cdot\left[\mu\left(\nabla\vec{v} + \nabla\vec{v}^{\mathrm{T}}\right)\right] + \rho\vec{g} \tag{5}$$

$$\nabla\cdot\left(\rho C_p T\vec{v}\right) = \nabla\cdot(\lambda\nabla T) \tag{6}$$

where C_p is the specific heat, g is the gravity acceleration, p is the pressure, T is the temperature, $\vec{v}$ is the velocity vector, ρ is the density, λ is the thermal conductivity.

In order to perform the comparison between BT (bare tube) and MHTT, a BT with a diameter of D and length of L is simulated (see Fig. 2(a)). The tube entrance ($x = 0$) has the following velocity profile:

$$u = 2u_{ave}\left[1 - \left(\frac{2r}{D}\right)^2\right] \tag{7}$$

where u_{ave} is the average velocity in the tube. The Reynolds number characterizing the flow and heat transfer is

$$Re = \frac{\rho D u_{ave}}{\mu} \tag{8}$$

Once Re is given, the inlet average velocity u_{ave} can be defined. The fluid temperature T_{in} is given at the tube inlet.

Fig. 2(b) shows the computation domain for MHTT. The tube diameter is also D. A bare tube section with its length of L_b was set. The modulated flow section has the length of L_m. The original point o($x = 0$, $r = 0$) was at the start of the mesh cylinder. The mesh cylinder upstream has negative x values. Different from the bare tube shown in Fig. 2(a), the uniform heat flux was applied only on the modulated flow section of L_m. The bare tube section was non-heated. Due to the geometry symmetry, only half of the circular tube was computed. For the BT (see Fig. 2(a)), $D = 13.8$ mm, $L = 1000.0$ mm. For the MHTT, $D = 13.8$ mm, $D_m = 10.0$ mm, $L_b = 200.0$ mm and $L_m = 1000.0$ mm.

Boundary conditions (BCs) for the BT are summarized as follows (see Fig. 2(a)):

inlet BC at $x = 0$: $u = u$ given by Eq. (7), $v = 0$, $T = T_{in}$;
outlet BC at $x = L$: $p = 1.013 \times 10^5$ Pa;
BC at the wall: $u = v = 0$, $q = q_w$.

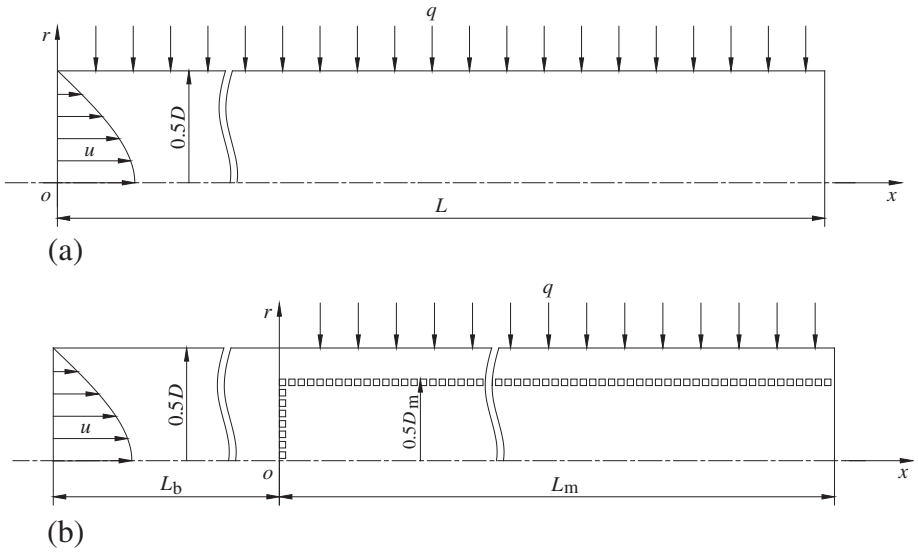

Fig. 2. The computation domain and boundary conditions (a for bare tube, b for modulated heat transfer tube).

BCs for the MHTT are summarized as follows (see Fig. 2(b)):
inlet BC: at $x = -L_b$, $u = u$ given in Eq. (7), $v = 0$, $T = T_{in}$;
outlet BC at $x = L_b + L$: $p = 1.013 \times 10^5$ Pa;
BC at the wall: $u = v = 0$; $q = 0$ within $-L_b < x < 0$ and $q = q_w$ within $0 < x < L_m$.

where u and v are the velocity component in axial flow direction and radial direction, respectively.

It is noted that mesh screens for MHTT have micron scale. The no-slip BCs of $u = v = 0$ are applied on each mesh wire surface. Because the mesh cylinder surface has a thin layer thickness of 85 μm, it is assumed that there is no apparent temperature gradient across the mesh wire thickness of 85 μm. Therefore, the thermal insulation BC was applied on each mesh wire surface:

$$\left.\frac{\partial T}{\partial n}\right|_{\text{mesh wall}} = 0 \tag{9}$$

where n is the unit vector perpendicular to the mesh wall surface.

3.3. Grid generation

MHTT behaves the strong multiscale characteristics, generating great difficulties on numerical simulations. A non-uniform grid generation system was developed (see Fig. 3), which was summarized as follows.

- A quasi-uniform grid size of 375 μm is applied along the axial flow direction (not including the near-mesh-pore region);
- A non-uniform grid sizes are used along the radial direction, with the coarse grid size of 375 μm in the bulk region, and the finest grid size of 25 μm for the first layer of the tube wall. The grids are gradually refined from the bulk region to the near wall region.
- Grid sizes are significantly refined near mesh pores. In order to adapt the grid size from the bulk region to the near-mesh-pore region, grid sizes are refined by two steps, with fine grid size of 21.25 × 16.25 μm near and within mesh pores, moderate grid size of 75 × 75 μm away from the mesh pores, and the normal grid size of 375 × 375 μm in the bulk region. The fine grid size of 21.25 × 16.25 μm corresponds to sixteen girds within a mesh pore.

3.4. Solution strategies

The commercial software (FLUENT 6.3.26 version) solved Eqs. (4)–(6) subjected to related boundary conditions. A processor Gambit 2.2.3 creates the computation domain for solver. The governing equations are discretized by the finite volume method. The SIMPLE algorithm deals with the coupling of pressure and velocity. The second order upwind scheme was applied for the momentum and energy conservation equations. Because the flow and heat

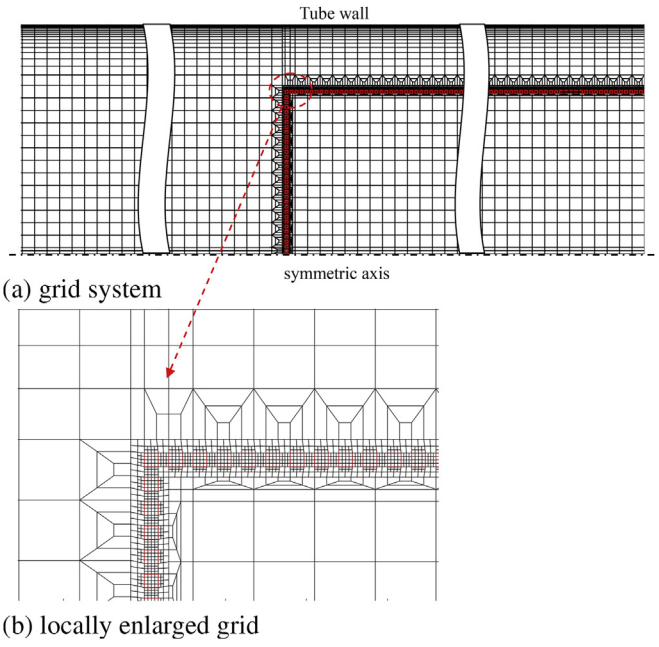

Fig. 3. The multiscale grid generation system.

transfer are coupled with each other, Eqs. (4)–(6) are solved alternatively. The under-relaxation factor was in the range of 0.2–0.8, with larger factor values for BT and smaller factor values for MHTT. Because the inserted mesh cylinder creates many refined mesh grids in micron scale, the residual error was set as 10^{-15}, which is significantly smaller than those in the literature. The computation was converged if the residual error for tracking parameters is less than 10^{-15}. The simulations were run on a work station having two 8-core CPUs (2.4 GHz each) and 24 GB of RAM. The computation needs about 2 h for each run of the MHTT computation.

4. Results and discussion

4.1. General heat transfer characteristic

The computation uses the non-slip boundary condition on the wall ($u_w = 0$ for this application). During the computation, the first fluid layer has a grid size of $y = 25$ μm on the wall, which was assumed to be stationary. The wall heat flux should be conducted through the fluid layer. The fluid temperature within the sub-layer was recorded as T_{grid}. The Fourier heat conduction law yields

$$q = -\lambda \left.\frac{\partial T}{\partial r}\right|_{r=R} \tag{10}$$

Thus T_w (wall temperature) was computed as

$$T_w = \frac{qy}{\lambda} + T_{grid} \tag{11}$$

where $y = 25 \times 10^{-6}$ m. The local Nusselt number was computed as

$$Nu_x = \frac{q}{T_w - T_f} \times \frac{D}{\lambda} \tag{12}$$

where T_f is the bulk fluid temperature, which is defined as

$$T_f = \frac{\int \rho C_p u T \, dA}{\int \rho C_p u \, dA} \tag{13}$$

The overall average Nusselt number is defined as

$$Nu_{ave} = \frac{q}{T_{w,ave} - T_{f,ave}} \times \frac{D}{\lambda} \tag{14}$$

where the average fluid temperature is $T_{f,ave} = 0.5(T_{in} + T_{out})$, $T_{w,ave}$ is the average wall temperature, which is computer as

$$T_{w,ave} = \frac{\sum_{i=1}^{n'} T_w}{n'} \tag{15}$$

where n' is the number of data points of wall temperature at the heating section.

Table 1 shows the 24 runs calculated in this study. Comparative runs were set for BT and MHTT run by run. Water was used as the working fluid. In order to neglect effect of physical property variation of water on the flow and heat transfer, the heat flux was arranged so that the bulk water temperature difference between inlet and outlet equals to 10.0 K for each run, i.e., $T_{out} - T_{in} = 10.0$ K. For BT, the numerical simulation gave perfect Nusselt number distribution along the flow length in both the thermal developing and developed regions, which are consistent with the classical solutions reported in Ref. [13]. For MHTT, the present simulation was independent of grid sizes when the grid sizes described in Section 3.3 were further refined.

Table 1
Runs computed for BT and MHTT.

Runs	Tubes	u_{ave} (m/s)	Re	q (w/m^2)	T_{in} (K)	T_{out} (K)	ΔT (K)
1	BT	0.0065	100	930.27	293.15	303.15	10.0
2	MHTT	0.0065	100	930.27	293.15	303.15	10.0
3	BT	0.0129	200	1860.55	293.15	303.15	10.0
4	MHTT	0.0129	200	1860.55	293.15	303.15	10.0
5	BT	0.0194	300	2790.82	293.15	303.15	10.0
6	MHTT	0.0194	300	2790.82	293.15	303.15	10.0
7	BT	0.0259	400	3721.09	293.15	303.15	10.0
8	MHTT	0.0259	400	3721.09	293.15	303.15	10.0
9	BT	0.0323	500	4651.36	293.15	303.15	10.0
10	MHTT	0.0323	500	4651.36	293.15	303.15	10.0
11	BT	0.0388	600	5581.64	293.15	303.15	10.0
12	MHTT	0.0388	600	5581.64	293.15	303.15	10.0
13	BT	0.0453	700	6511.91	293.15	303.15	10.0
14	MHTT	0.0453	700	6511.91	293.15	303.15	10.0
15	BT	0.0517	800	7442.18	293.15	303.15	10.0
16	MHTT	0.0517	800	7442.18	293.15	303.15	10.0
17	BT	0.0582	900	8372.45	293.15	303.15	10.0
18	MHTT	0.0582	900	8372.45	293.15	303.15	10.0
19	BT	0.0647	1000	9302.73	293.15	303.15	10.0
20	MHTT	0.0647	1000	9302.73	293.15	303.15	10.0
21	BT	0.0712	1100	10,233.00	293.15	303.15	10.0
22	MHTT	0.0712	1100	10,233.00	293.15	303.15	10.0
23	BT	0.0776	1200	11,163.27	293.15	303.15	10.0
24	MHTT	0.0776	1200	11,163.27	293.15	303.15	10.0

Fig. 4 shows Nusselt numbers and wall temperatures along the flow length x at $Re = 100$ and 1000. The Nusselt number of 4.36 for

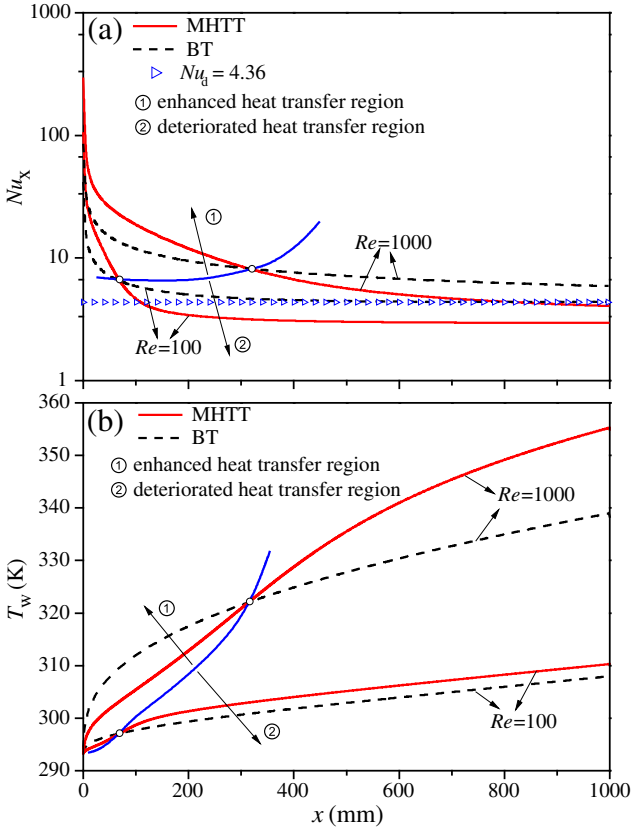

Fig. 4. Comparisons of local Nusselt numbers and wall temperatures between bare tube and modulated heat transfer tube ($Re = 100$ refers to run 1 for BT and run 2 for MHTT, $Re = 1000$ refers to run 19 for BT, and run 20 for MHTT, see Table 1).

the thermally developed heat transfer was marked, indicating that the thermal developed heat transfer can be reached at $Re = 100$ but cannot be reached at $Re = 1000$, with the heating length of 1000.0 mm. We note that Nu_x was plotted in a logarithm way. The solid-red (in the web version) and dashed-black curves represent the results for MHTT and BT, respectively. The red (in the web version) and black curves are intercrossed at each Reynolds number, with the junction point strongly dependent on Re (see Fig. 4). For example, the junction point appears at $x = 68.6$ mm with $Re = 100$, but it is shifted to $x = 312.0$ mm with $Re = 1000$. The high Reynolds number delays the junction point to occur. In terms of the junction point, the flow and heat transfer behavior is divided into two different regions: the enhanced heat transfer region before the junction point, and the deteriorated heat transfer region beyond the junction point. The blue (in the web version) curves in Fig. 4 connect the junction points for cases with different Reynolds numbers, distinguishing the enhanced heat transfer region and deteriorated heat transfer region. In the enhanced heat transfer region, Nusselt numbers are larger for MHTT than those for BT, and wall temperatures are lower for MHTT than those for BT (see Fig. 4(a)–(b)). Inversely, MHTT has poorer thermal performance than BT, in the deteriorated heat transfer region.

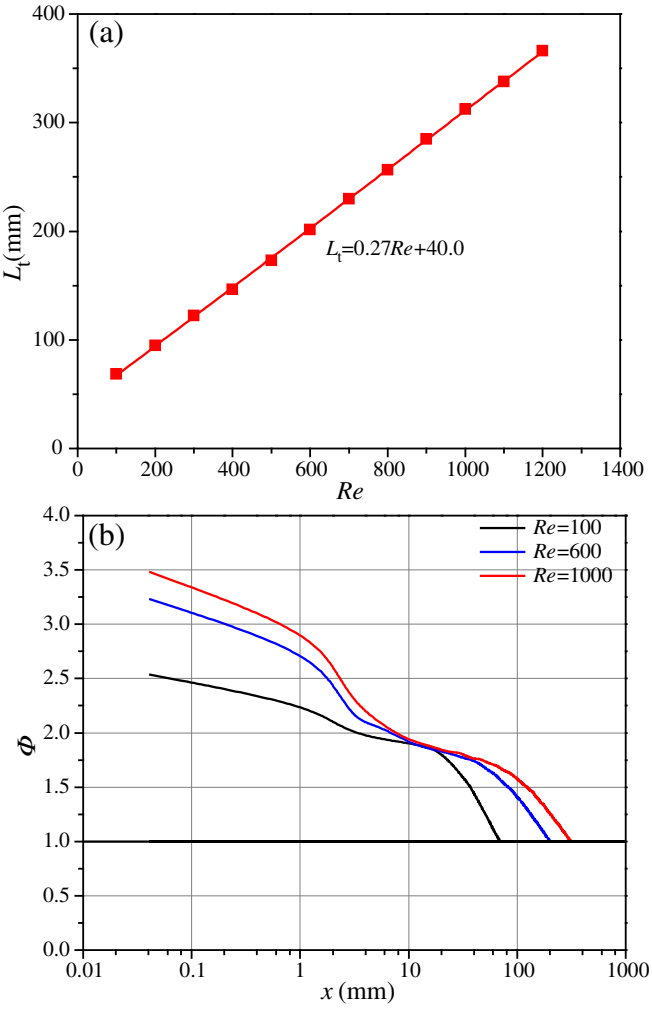

Fig. 5. The transition flow lengths from enhanced heat transfer to deteriorated heat transfer versus Reynolds numbers (a) and the enhanced heat transfer factors versus axial flow length (b).

A transition flow length (L_t) was defined as that from $x = 0$ to the junction point. Fig. 5(a) shows a perfect linear relationship between L_t and Re, which is

$$L_t = 0.27Re + 40.0 \tag{16}$$

where L_t has the unit of millimeter. It is noted that L_t should be influenced by tube and mesh cylinder dimensions and working fluids.

Local enhanced heat transfer factor (ϕ) is defined as the Nusselt number for MHTT divided by that for BT. Fig. 5(b) shows ϕ versus x. In the enhanced heat transfer region, ϕ is significantly larger than one, but decreased along the flow direction. Reynolds numbers strongly influence ϕ. The higher the Reynolds number, the larger the enhanced heat transfer factor is. The maximum ϕ attains 3.5 at $Re = 1000$. The critical condition at $\phi = 1$ corresponds to the junction point shown in Fig. 4.

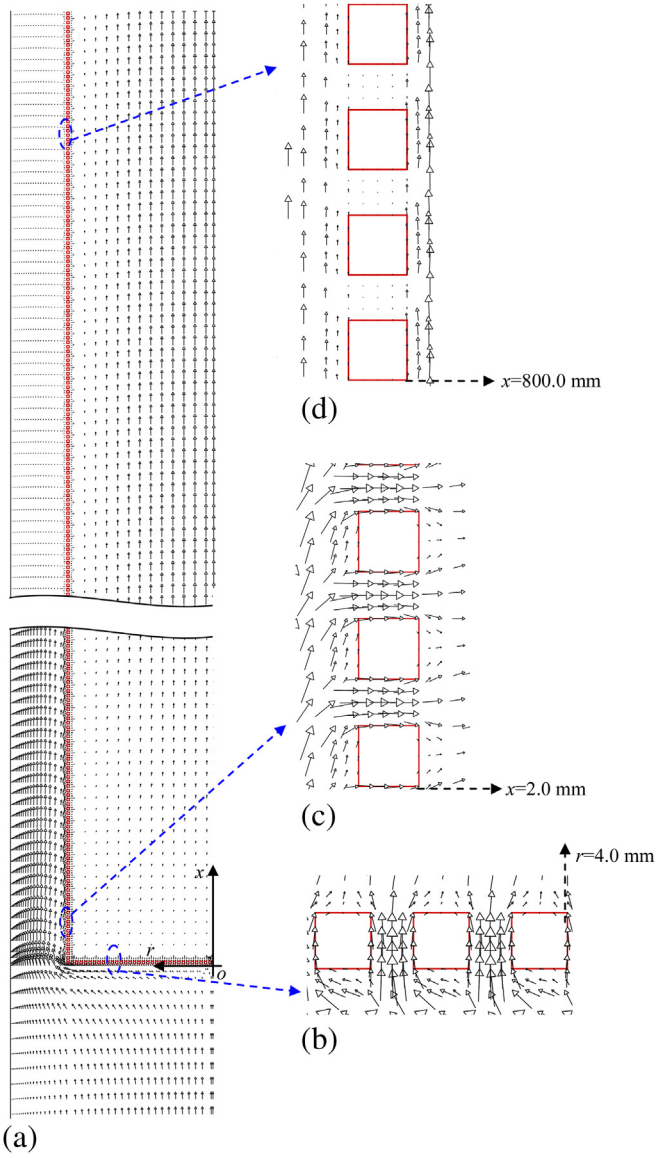

Fig. 6. The flow field over the computation domain and the enlarged flow fields at $Re = 100$, run 2, see Table 1.

4.2. Flow and heat transfer behavior at Re = 100

Fig. 6(a) shows the flow field over the whole MHTT length. Enlarged flow fields near mesh pores are plotted at three axial locations of $x = 0$, 2.0 mm and 800.0 mm (see Fig. 6(b)–(d)). Fig. 6(b) shows the distorted near-mesh-pore field at $x = 0$. When a fluid stream strikes the mesh screen, part of the flow rate enters the core region through mesh pores. But most of the flow rate flows in the annular region, creating larger velocity and its gradient near the wall to enhance heat transfer. With the flow evolution in the downstream, flow from the annular region to the core region occurs, causing the decreased velocity and velocity gradient in the annular region (see Fig. 6(c)). When the flow is far away from the mesh cylinder entrance, the flows become parallel in the annular region and core region (see Fig. 6(d)). The velocity and velocity gradient become smaller than those in the bare tube, thus the heat transfer is deteriorated. Fig. 7 highlights the flow fields in four specific regions. These figures show the larger velocity and velocity gradient in the annular region, but they are decreased along the flow direction, until the critical condition appears at $x = 68.6$ mm. The flow in the annular region becomes weak at $x = 800.0$ mm.

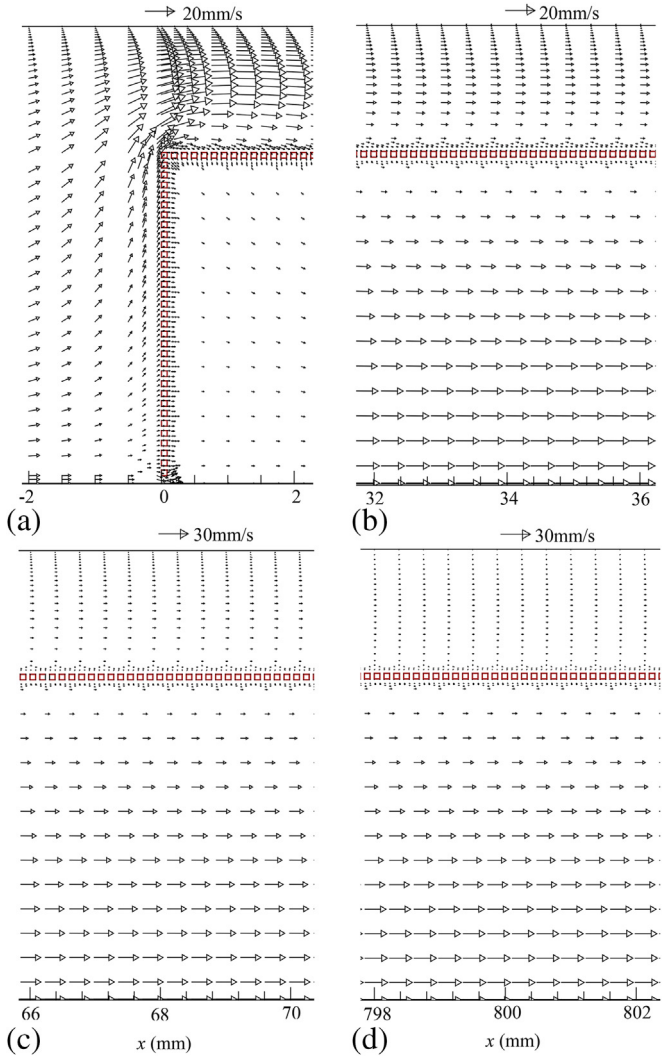

Fig. 7. Local flow field at different locations at $Re = 100$ (a: fluid stream striking the bottom mesh screen, b: enhanced heat transfer region, c: transition region at which $\phi = 1$, d: deteriorated heat transfer region, run 2, see Table 1).

Fig. 8 shows the axial velocity and temperature distribution over the tube cross section at three specific locations. The red and black curves are for MHTT and BT, respectively. For MHTT, the axial velocities behave the double-peak distribution, with one peak in the annular region and the other one at the tube center of $r = 0$ (see left row of Fig. 8). At the mesh cylinder surface ($r = 0.5D_m$), axial velocities approach zero due to the non-slip BCs applied there.

4.2.1. Enhanced heat transfer region (Fig. 8(a) and (d))

Indeed a large velocity and velocity gradient exist near the wall for MHTT (see Fig. 8(a)). The peak velocity in the annular region for MHTT is greatly larger than the velocities near the wall for BT. The peak velocity at the tube center ($r = 0$) for MHTT is slightly smaller than that for BT. The velocity distribution yields larger flow rate in the annular region and smaller flow rate in the core region, which is perfect for the heat transfer enhancement. Examining right row of Fig. 8 identifies the thinned thermal boundary layer thickness for MHTT. Wall temperatures are lower for MHTT than those for BT.

4.2.2. Critical condition with $\phi = 1$ (Fig. 8(b) and (e))

The critical condition refers to $\phi = 1$. Both the velocity gradient and temperature gradient near the wall are the same for MHTT and BT. Wall temperatures are exactly the same for MHTT and BT.

4.2.3. Deteriorated heat transfer region (Fig. 8(c) and (f))

The flow in the annular region becomes weak for MHTT. Most of the flow rate flows in the core region, with the peak velocity at $r = 0$ significantly larger than that for BT. Wall temperatures are larger for MHTT than those for BT.

4.3. Flow and heat transfer behavior at Re = 1000

Figs. 9–11 demonstrate results at $Re = 1000$. Qualitatively, flow and heat transfer in the enhanced heat transfer region, critical condition and deteriorated heat transfer region are identical to those at $Re = 100$. The velocity and velocity gradient are larger near the wall for MHTT than those for BT. The thermal boundary layer is thinner for MHTT than that for BT. At the critical condition, the same velocity and velocity gradient occur near the wall for MHTT and BT. Wall temperatures are identical for both tubes. In the deteriorated heat transfer region, the flow stream becomes parallel between the annular region and core region. Flow in the annular region is weak because most of the flow rate enters the core region through mesh pores. The deteriorated heat transfer region possesses higher wall temperatures and lower heat transfer coefficients. The transition flow length is linearly increased with increases in Reynolds numbers, which becomes 312.0 mm at $Re = 1000$.

4.4. The improved modulated heat transfer tube

Suspending a mesh cylinder in a tube increases velocity and its gradient near the wall. The thermal boundary layer is also thinned. Continuous flow through mesh pores decreases the velocity and velocity gradient near the wall to yield a critical condition at which the enhanced heat transfer factor equals to one, beyond which the heat transfer is deteriorated. This finding inspired us to use short mesh cylinder suspended in the tube to ensure that the critical condition is not reached. Fig. 12 shows an example design, which is the same as that shown in Fig. 2(b), except that eight short mesh cylinders are suspended within a heating length of $L_m = 1000.0$ mm. Each mesh cylinder has the same diameter of D_m as that shown in Fig. 2(b), but has a short length of $L_{m'} = 100.0$ mm. The distance between two neighboring mesh cylinders was $L_{b'} = 25.0$ mm. The idea is to create repeated flow fields with larger

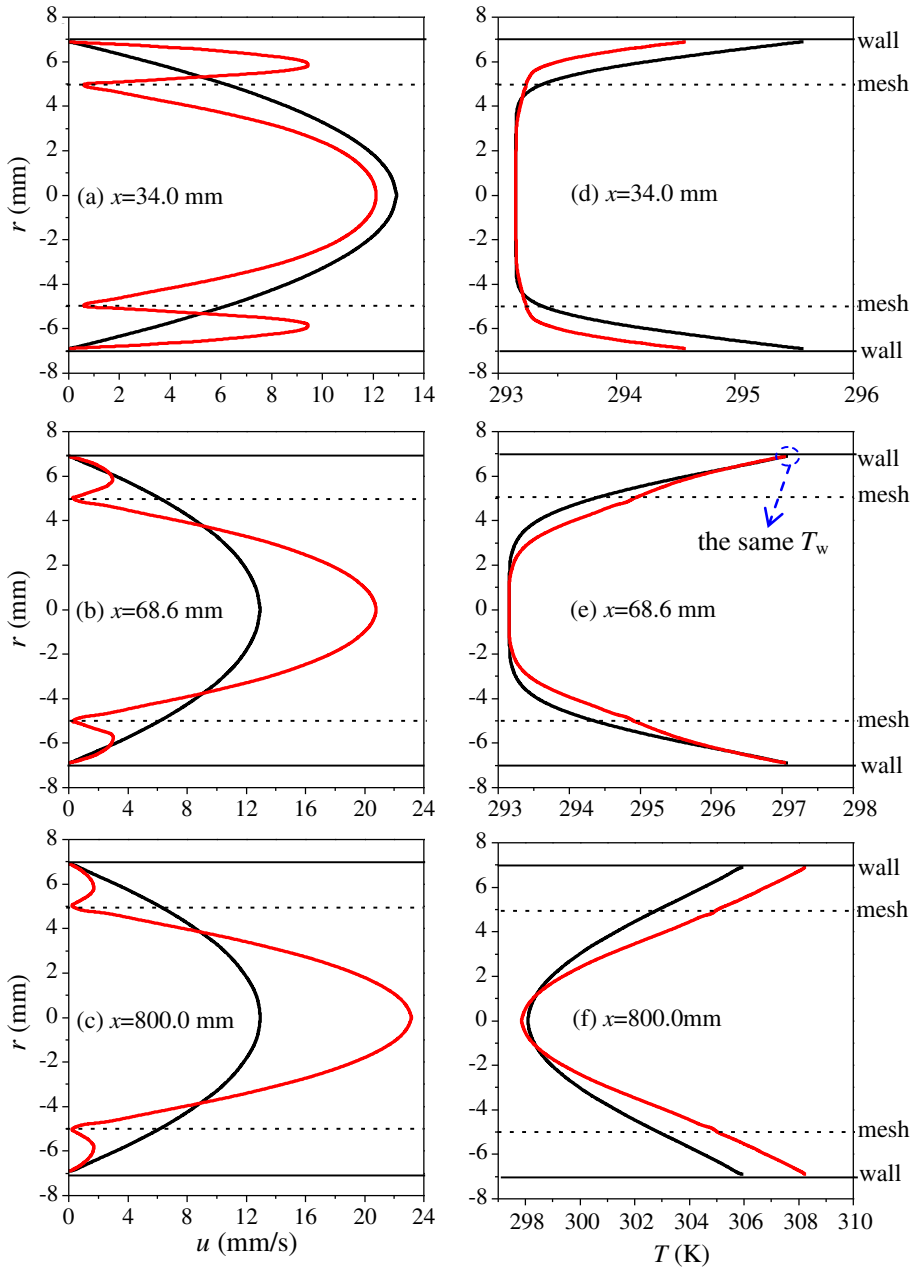

Fig. 8. Axial velocities and fluid temperatures over the tube cross section at different axial locations at $Re = 100$ (black and red curves for bare tube and modulated heat transfer tube respectively, runs 1 and 2, see Table 1). (For interpretation of the references to color in this figure legend, the reader is referred to the web version of this article.)

velocity and velocity gradient near the wall. When the fluid stream at the former mesh cylinder exit strikes the next mesh cylinder, the flow field is redistributed. Due to the short mesh cylinder used, the critical condition at which $\phi = 1$ is never reached. The invention is called the improved modulated heat transfer tube (IMHHT). Table 2 shows the 20 runs computed for BT and IMHHT.

Fig. 13 shows wall temperatures, Nusselt numbers and enhanced heat transfer factors versus flow length, in which solid and dashed curves are for IMHTT and BT, respectively. The heat transfer characteristics behave the periodic behavior. Wall temperatures are significantly lower for IMHTT than those for BT. IMHTT decreases wall temperatures by 4.68 K and 11.06 K at $x = 1000$ mm for $Re = 600$ and 1000, respectively (see Fig. 13(a)). Nusselt numbers are always larger for IMHTT than those for BT (see Fig. 13(b)). Fig. 13(c) demonstrates the enhanced heat transfer factors, displaying the cycle behavior. The enhanced heat transfer factors depend on Reynolds numbers. The higher the Reynolds number, the larger heat transfer enhancement degree is. In contrast to a single long mesh cylinder suspended in the tube, suspending a set of short mesh cylinders increases the Nusselt numbers over the whole flow length. The critical condition never happens. Fig. 14 examines the flow field. Indeed the flow fields are periodically repeated. Because there are eight mesh cylinders in the tube, we focus on the flow field for part 2. In contrast to MHTT, IMHTT has apparent fluid velocity and its gradient near the wall before the fluid stream strikes the next mesh cylinder section. This accounts for the heat transfer enhancement mechanism for IMHTT. Fig. 15 shows the average Nusselt numbers and enhanced heat transfer factors. The heat transfer enhancement degree is strongly dependent on Reynolds number. The larger the Reynolds number, the

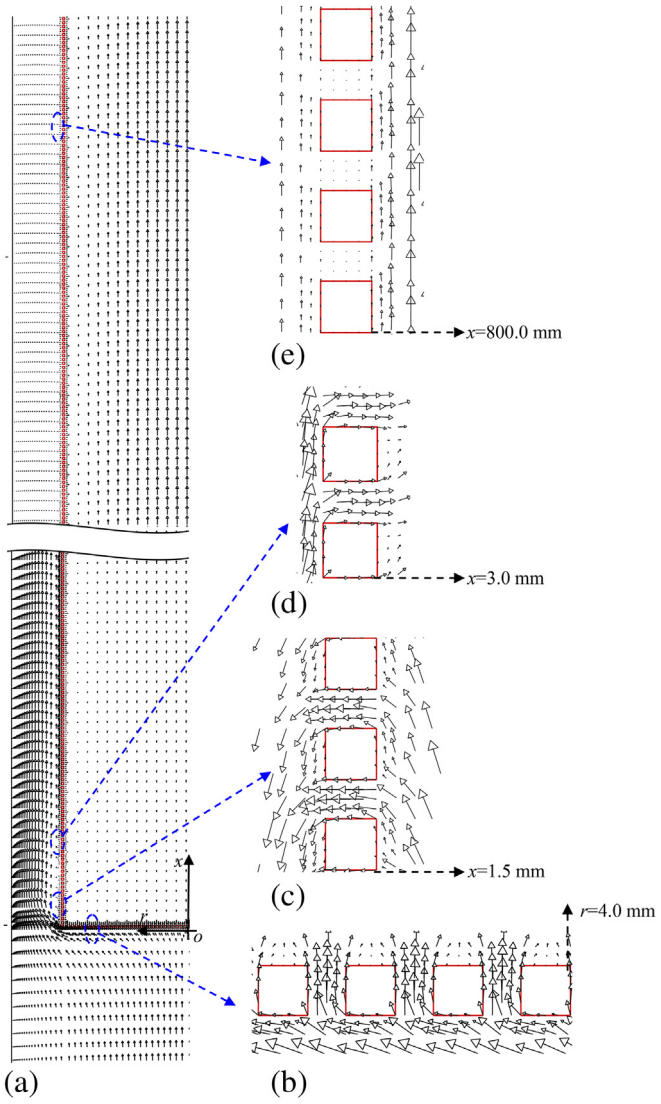

Fig. 9. Flow field over the whole computational domain and enlarged flow field for $Re = 1000$, run 20, see Table 1.

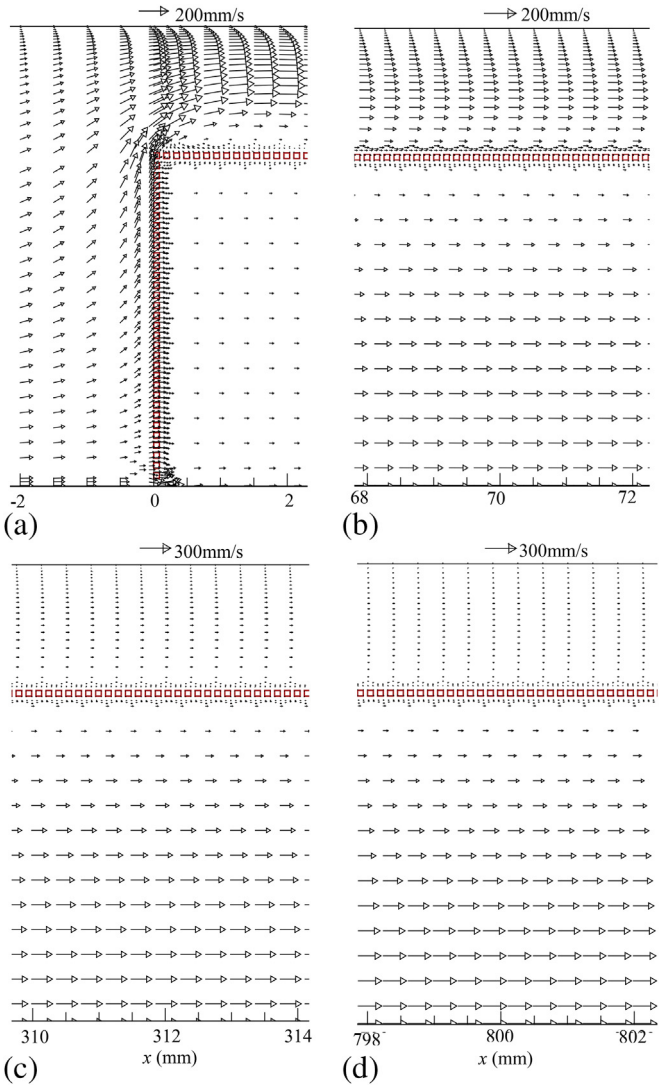

Fig. 10. Local flow field at different locations at $Re = 1000$ (a: fluid stream striking the bottom mesh screen, b: enhanced heat transfer region, c: transition region at which $\phi = 1$, d: deteriorated heat transfer region, run 20, see Table 1).

higher heat transfer enhancement factor is. At $Re = 1000$, the heat transfer enhancement factor attains 1.73.

4.5. Validation by the experiments

To validate the reliability of the numerical method, an experiment was performed. The deionized/degassed water was the working fluid. A forced convective loop was built to supply constant flow rate to a stainless steel tube, which was regarded as the test section. The test tube is either a bare tube (BT) or a modulated heat transfer tube (MHTT). It has the same geometry configuration and dimensions as shown in Fig. 2 for numerical simulations. The test tube was vertically positioned and directly heated by the DC (direct current). It was well thermally insulated. The net heat flux on the inner wall of the test tube is decided by the fluid enthalpy increment between inlet and outlet divided by the inner wall surface area of the tube. The mass flow rate was measured by a mass flow meter with its accuracy of 0.2%. Two K-type jacket thermocouples measured the inlet and outlet fluid temperatures. Thirteen thermocouple wires were soldered on the outer wall of the test tube, which had the accuracy of 0.2 °C. The inner wall temperature was computed as [14]

$$T_w = T_{wo} - \frac{qD}{4\lambda_w} \times \frac{\left(\frac{D}{D_o}\right)^2 - 2\ln\left(\frac{D}{D_o}\right) - 1}{1 - \left(\frac{D}{D_o}\right)^2} \tag{17}$$

where T_w is the inner wall temperature, T_{wo} is the measured outer wall temperature, D and D_o are the inner and outer tube diameters respectively, λ_w is the tube wall thermal conductivity. The local Nusselt number is defined as

$$Nu_x = \frac{qD}{\lambda\left(T_w - T_f\right)} \tag{18}$$

where λ is the fluid thermal conductivity and T_f is the fluid temperature over the tube cross section at axial length x.

In our experiment, the fluid physical properties are assumed constant. The experimental uncertainties for Re and Nu are estimated by a random uncertainty propagation technique. The

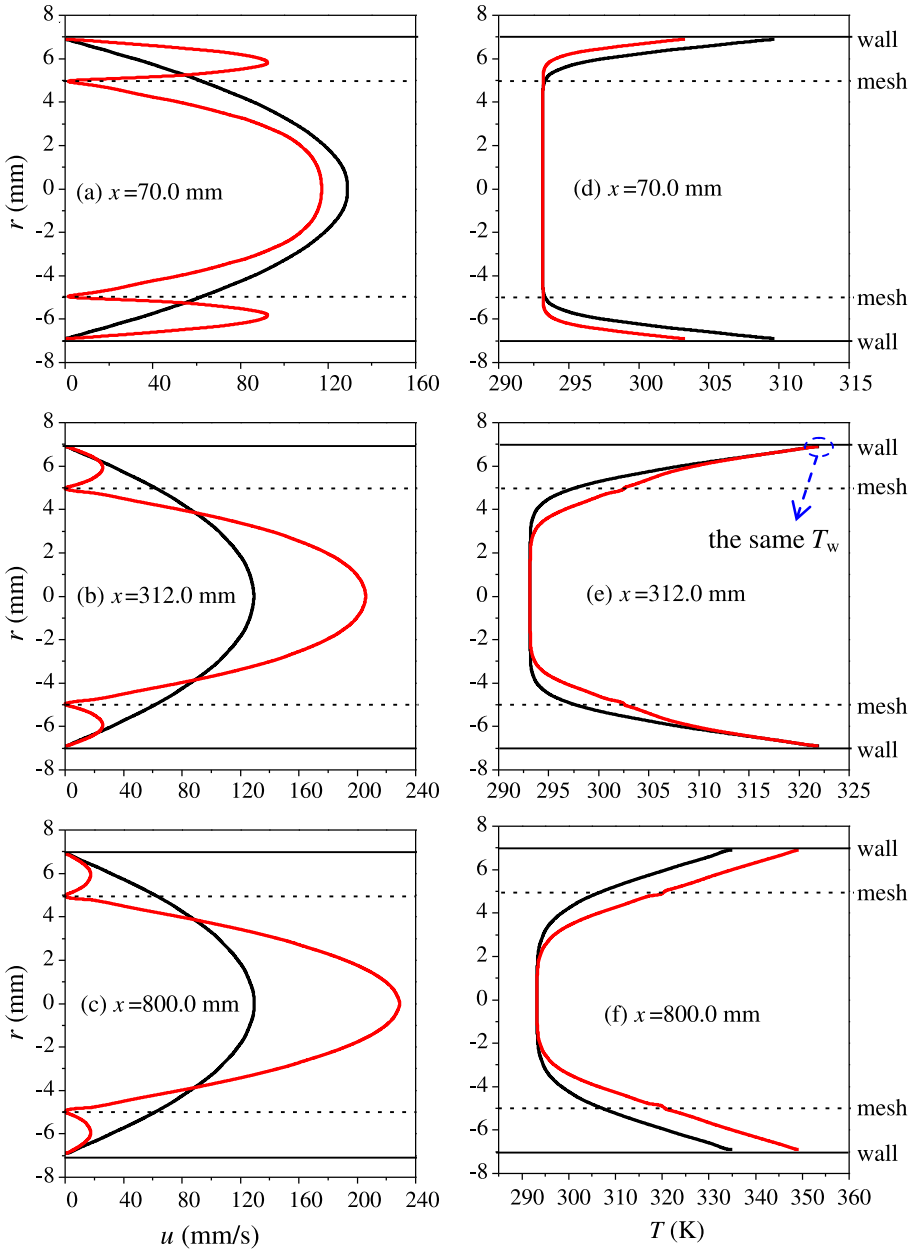

Fig. 11. Axial velocities and fluid temperatures over the tube cross section at different axial locations (Re = 1000, black and red curves for bare tube and modulated heat transfer tube, runs 19 and 20, see Table 1). (For interpretation of the references to color in this figure legend, the reader is referred to the web version of this article.)

Re and *Nu* had the uncertainties of about 2.7% and 3.0%, respectively. Fig. 16(a) shows the MHTT tube structure. Fig. 16(b) and (c) shows the enlarged mesh screen and fabricated mesh cylinder.

This is a preliminary study regarding the modulated heat transfer. Preliminary experimental data were achieved in laminar flow regime. Fig. 17 shows the measured wall temperatures and Nusselt numbers against computed values at Re = 1000. It is seen

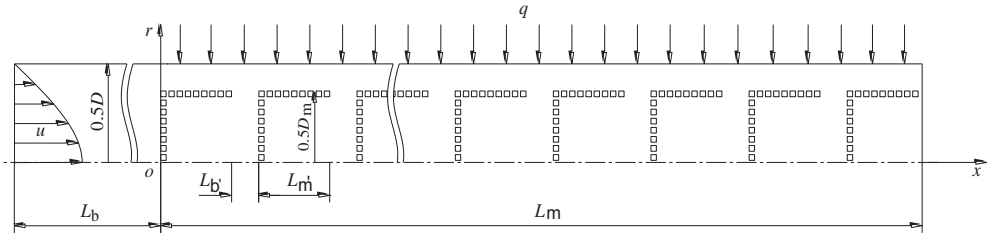

Fig. 12. The computation domain with a set of short mesh cylinders inserted.

Table 2
Runs computed for BT and IMHTT.

Runs	Tubes	u_{ave} (m/s)	Re	q (w/m^2)	T_{in} (K)	T_{out} (K)	ΔT (K)
1	BT	0.0065	100	930.27	293.15	303.15	10.0
2	IMHTT	0.0065	100	930.27	293.15	303.15	10.0
3	BT	0.0129	200	1860.55	293.15	303.15	10.0
4	IMHTT	0.0129	200	1860.55	293.15	303.15	10.0
5	BT	0.0194	300	2790.82	293.15	303.15	10.0
6	IMHTT	0.0194	300	2790.82	293.15	303.15	10.0
7	BT	0.0259	400	3721.09	293.15	303.15	10.0
8	IMHTT	0.0259	400	3721.09	293.15	303.15	10.0
9	BT	0.0323	500	4651.36	293.15	303.15	10.0
10	IMHTT	0.0323	500	4651.36	293.15	303.15	10.0
11	BT	0.0388	600	5581.64	293.15	303.15	10.0
12	IMHTT	0.0388	600	5581.64	293.15	303.15	10.0
13	BT	0.0453	700	6511.91	293.15	303.15	10.0
14	IMHTT	0.0453	700	6511.91	293.15	303.15	10.0
15	BT	0.0517	800	7442.18	293.15	303.15	10.0
16	IMHTT	0.0517	800	7442.18	293.15	303.15	10.0
17	BT	0.0582	900	8372.45	293.15	303.15	10.0
18	IMHTT	0.0582	900	8372.45	293.15	303.15	10.0
19	BT	0.0647	1000	9302.73	293.15	303.15	10.0
20	IMHTT	0.0647	1000	9302.73	293.15	303.15	10.0

that the present numerical simulations matched the experimental measurements reasonably in laminar flow regime. It is noted that engineering applications need turbulent flow in tubes under many situations. Fig. 18 shows the measured wall temperatures and

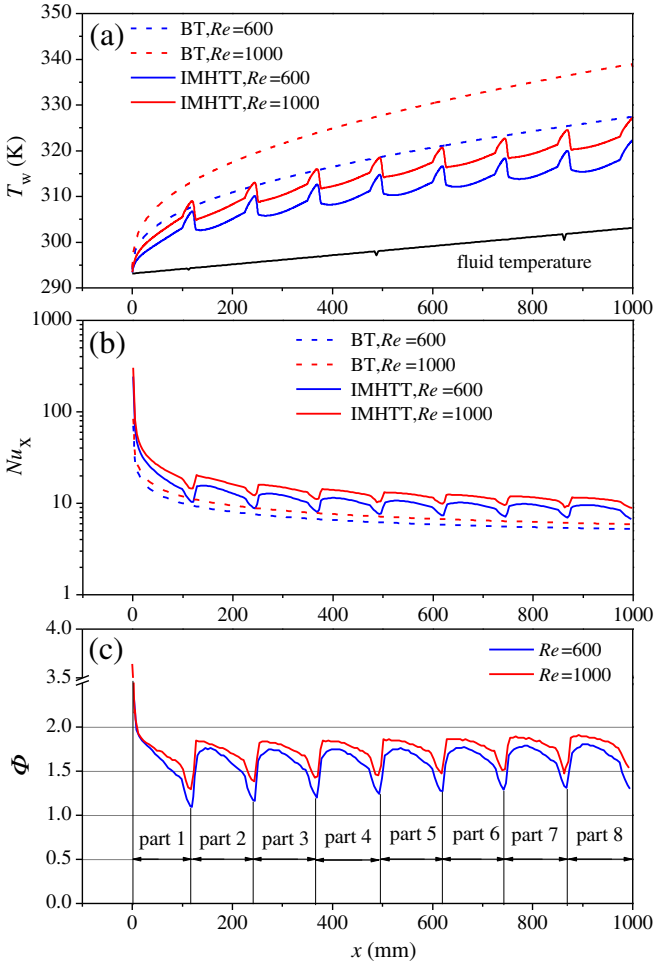

Fig. 13. Wall temperatures, Nusselt numbers and enhanced heat transfer factors versus axial flow lengths at Re = 600 for run 12 and 1000 for run 20 (see Table 2).

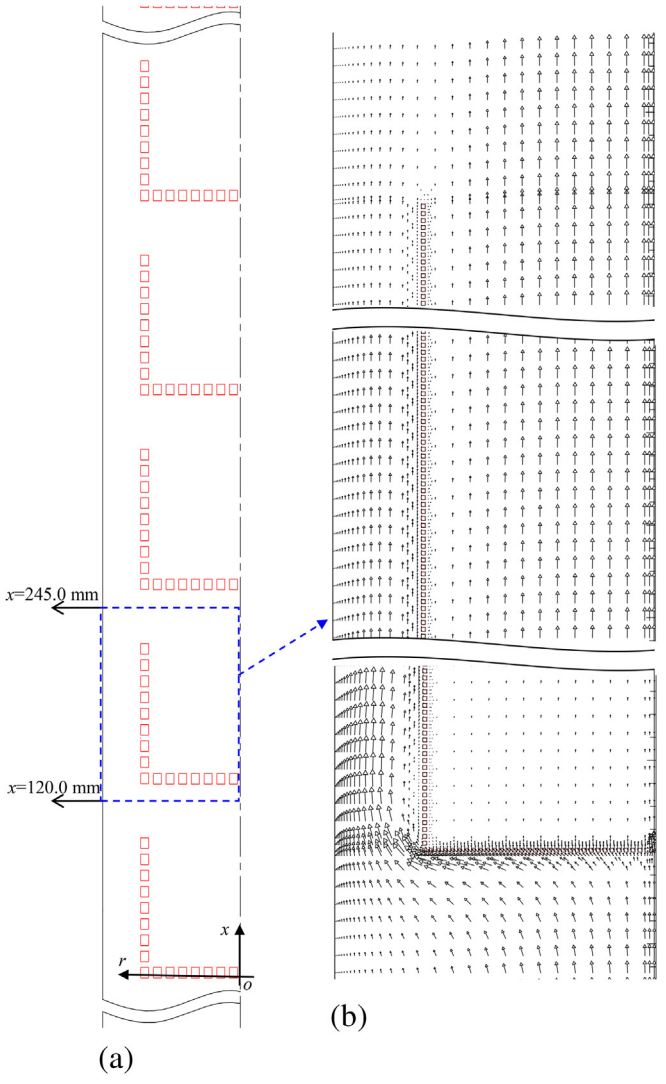

Fig. 14. The typical flow field for the improved modulated heat transfer tube (IMHTT, run 20 in Table 2).

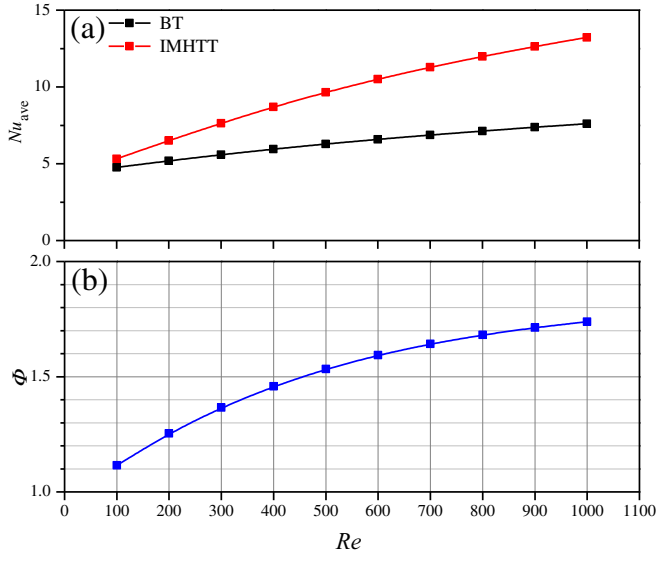

Fig. 15. The bulk averaged Nusselt number and enhance heat transfer factors versus Reynolds number.

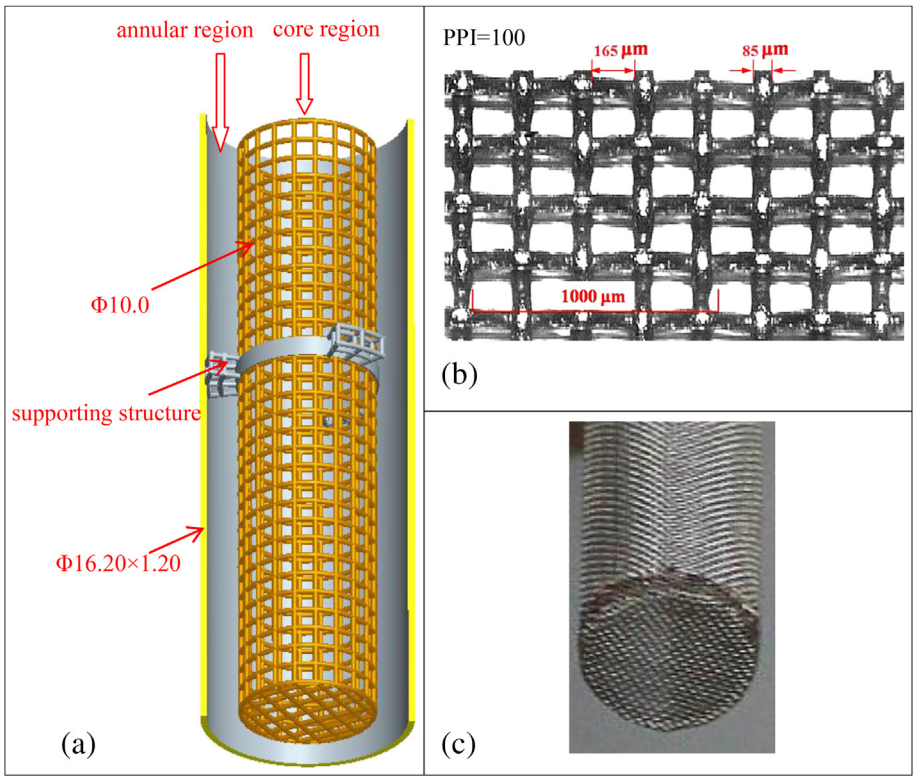

Fig. 16. The enhanced heat transfer tube with mesh cylinder inserted (a), photo of mesh screen (b) and the fabricated mesh cylinder (c).

Nusselt numbers for bare tube (BT) and modulated heat transfer tube (MHTT) in turbulent flow regime. The Reynolds numbers are almost identical with $Re = 14{,}176$ for BT and $Re = 14{,}182$ for MHTT. The heat flux was about 200 kW/m^2. It is seen that the MHTT can decrease the wall temperatures by more than 10–15 °C under similar running parameters (see Fig. 18(a)). Correspondingly, the Nusselt numbers are significantly larger for MHTT than those for BT (see Fig. 18(b)). It is noted that a supporting structure is located at about $x = 0.5$ m, corresponding to the more decreased wall temperature and higher Nusselt number there for MHTT. In summary, the preliminary study demonstrates that MHTT can enhance heat transfer not only in laminar flow regime, but also in turbulent flow regime. Detailed studies on mechanism and optimization of the MHTT are expected in the near future.

5. Conclusions

The following conclusions can be drawn:

- The flow field modulation concept was proposed. A mesh cylinder was suspended in the tube, creating an annular region

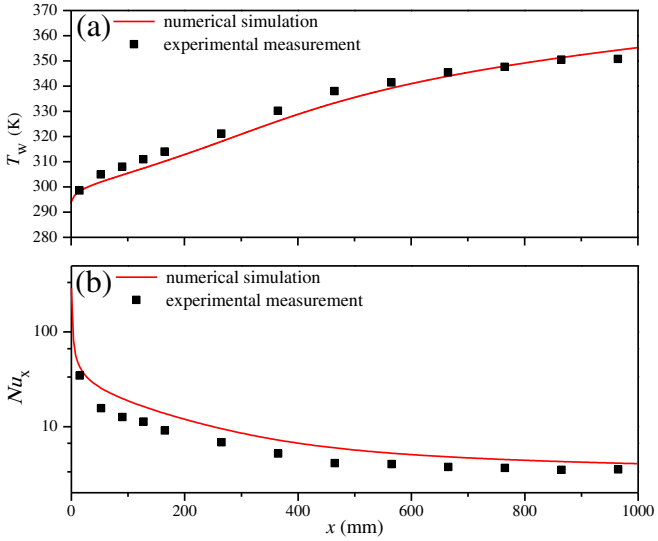

Fig. 17. Comparison of numerical and experimental results ($Re = 1000$, run 20, see Table 1).

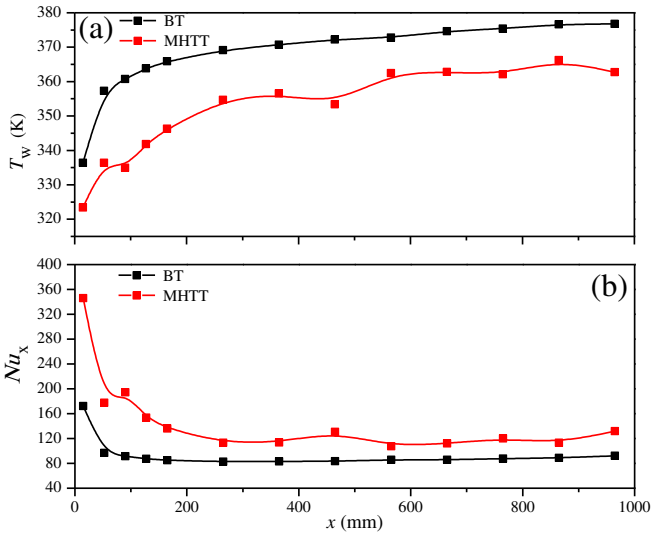

Fig. 18. Local wall temperature and Nusselt numbers versus axial flow direction (BT: $Re = 14{,}176$, $q = 200.31$ kW/m^2; MHTT: $Re = 14{,}182$, $q = 200.21$ kW/m^2).

and a core region. An equal flow area criterion was developed for the 3D to 2D conversion of mesh pores. The numerical simulation was performed with non-uniform grid generation system, linking micron scale of mesh pores with macroscale of the tube.

- The results show the double-peak velocity distribution over the tube cross section. The invented tube generates increased velocity and its gradient near the wall. The thermal boundary layer is also thinned. Continuous flow through mesh pores decreases the velocity and velocity gradient near the wall to yield a critical condition at which the enhanced heat transfer factor equals to one, beyond which the heat transfer is deteriorated.
- The improved modulated heat transfer tube generates the periodic flow field and ensures the critical condition at which the heat transfer enhancement factor equals to one is never reached. Thus heat transfer is enhanced over the whole tube length.
- The numerical simulation results matched the measurements in laminar flow regime. The new tube also enhances heat transfer in turbulent flow regime. Mesh pore sizes and other related geometry dimensions are to be optimized in the future.

Acknowledgment

The work was supported by the Natural Science Foundation of China of International cooperation project (51210011), the National Basic Research Program of China (2011CB710703), the Natural Science Foundation of China of U1034004 and 51106049 and the Beijing Science and Technology development project (D121100004612005).

References

[1] A. Dewan, P. Mahanta, K.S. Raju, P.S. Kumar, Review of passive heat transfer augmentation techniques, Proc. Inst. Mech. Eng., A: J. Power Energy 218 (2004) 509–527.
[2] S. Liu, M. Sakr, A comprehensive review on passive heat transfer enhancements in pipe exchangers, Renew. Sust. Energy Rev. 19 (2013) 64–81.
[3] S. Eiamsa-Ard, C. Thianpong, P. Eiamsa-Ard, P. Promvonge, Convective heat transfer in a circular tube with short-length twisted tape insert, Int. Commun. Heat Mass Transf. 36 (2009) 365–371.
[4] J. Guo, A. Fan, X. Zhang, W. Liu, A numerical study on heat transfer and friction factor characteristics of laminar flow in a circular tube fitted with center-cleared twisted tape, Int. J. Therm. Sci. 50 (2011) 1263–1270.
[5] S. Saha, S.K. Saha, Enhancement of heat transfer of laminar flow of viscous oil through a circular tube having integral helical rib roughness and fitted with helical screw-tapes, Exp. Therm. Fluid Sci. 47 (2013) 81–89.
[6] S. Bhattacharyya, S. Saha, S.K. Saha, Laminar flow heat transfer enhancement in a circular tube having integral transverse rib roughness and fitted with centre-cleared twisted-tape, Exp. Therm. Fluid Sci. 44 (2013) 727–735.
[7] X.Y. Zhang, Z.C. Liu, W. Liu, Numerical studies on heat transfer and flow characteristics for laminar flow in a tube with multiple regularly spaced twisted tapes, Int. J. Therm. Sci. 58 (2012) 157–167.
[8] S. Eiamsa-ard, P. Promvonge, Thermal characteristics in round tube with serrated twisted tape, Appl. Therm. Eng. 30 (2010) 1673–1682.
[9] I. Kurtbas, F. Culcimen, A. Akbulut, D. Buran, Heat transfer augmentation by swirl generators inserted into a tube with constant heat flux, Int. Commun. Heat Mass Transf. 36 (2009) 865–871.
[10] P. Promvonge, Heat transfer behaviors in round tube with conical ring inserts, Energy Convers. Manage. 49 (2008) 8–15.
[11] P. Promvonge, S. Eiamsa-ard, Heat transfer enhancement in a tube with combined conical-nozzle inserts and swirl generator, Energy Convers. Manage. 47 (2006) 2867–2882.
[12] P. Naphon, M. Nuchjapo, J. Kurujareon, Tube side heat transfer coefficient and friction factor characteristics of horizontal tubes with helical rib, Energy Convers. Manage. 47 (2006) 3031–3044.
[13] L. Jia, Z.H. Fang, Advanced Heat Transfer, second ed., Higher Education Press, Beijing, 2008, pp. 181–185.
[14] R. Yun, Y. Kim, M. Soo Kim, Y. Choi, Boiling heat transfer and dryout phenomenon of CO_2 in a horizontal smooth tube, Int. J. Heat Mass Transf. 46 (2003) 2353–2361.